Theoretical photoemission line shapes and many body correlations

A. Bödicker and W. Schattke

Institut für Theoretische Physik, Universität Kiel
Leibnizstraße 15, 24118 Kiel, Germany

Angle resolved photoemission spectroscopy (ARPES) of high temperature superconductors has revealed an unusual behavior of line width and line shape, which has been interpreted as an indication for a Fermi liquid like ground state. The prototype for investigations of such ARPES line shapes in normal conductors is the isolated, strong and nearly non–dispersive Ti–3d derived emission near the Fermi level of the quasi twodimensional, metallic layer compound $TiTe_2$[1, 2]. Comparing experimental photoemission data only with the initial states spectral density, a decision in favor of a Fermi liquid is not fully conclusive. Furthermore, that comparison shows a deviation from the Fermi liquid behavior in the vicinity of the M point, because of neglecting band structure effects. In order to clarify this problem we performed full theoretical calculations of photoemission spectra within the onestep model. For the initial states standard parametrizations of the Fermi liquid selfenergy were chosen. The resulting energy distribution curves for several angles of emission are reported. In addition many body effects in the final states were considered by properly calculating the optical potential in the GW–approximation.

1 Introduction

Up to the present, angle resolved photoemission spectroscopy (ARPES) has been nearly exclusively used to investigate the occupied valence band structure neglecting all further information that the line shape of photoemission peaks possibly provides. The unusual behavior of the ARPES linewidths and line shapes of high temperature superconductors gave rise to line shape analyses to get a deeper insight into many particle interactions. In order to test the application of line shape analysis to photoemission spectra, a relatively simple case has to be chosen. The prototype for such investigations is the isolated, strong and nearly non–dispersive emission of $TiTe_2$ near the Fermi level along the ΓM–direction[1, 2]. Experimental ARPES spectra were fitted by a least squares method to a Fermi liquid type spectral function. In the region where the Ti–3d derived band crosses the Fermi level, excellent agreement between the experimental line shape and the Fermi level liquid model has been found. But there are conspicuous deviations between the theoretical and the experimental line shape at the Brillouin zone boundary. This situation gave rise to our calculations of photoemission spectra within the onestep model taking many body effects into account. After introducing the substance $TiTe_2$ and the photoemission theory, our investigations on the many particle effects in the initial and the final states of photoemission are reported in chapter 2.

1.1 Titanium Ditelluride

1T–$TiTe_2$ is an experimentally well investigated semimetallic compound belonging to the family of transition metal dichalcogenides. Its crystal structure may be described as a stack of identical layers, loosely bound to each other across a van der Waals gap. Each layer consists of a sheet of titanium atoms, sandwiched by two sheets of tellurium atoms. This layer structure explains the pseudo–twodimensional nature of $TiTe_2$. Figure 1 shows the unit cells of the direct and reciprocal lattice. The (001) surface usually being prepared experimentally is created by cleaving the crystal along the van der Waals gap. $TiTe_2$ differs from other transition metal dichalcogenides in that no charge density wave induced phase transitions occur. Figure 2 shows the valence band structure.

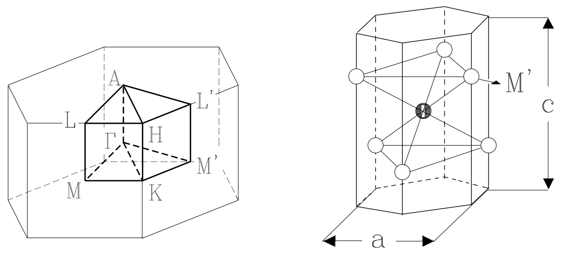

Figure 1: Unit cells of the direct (right) and reciprocal (left) lattice of $TiTe_2$

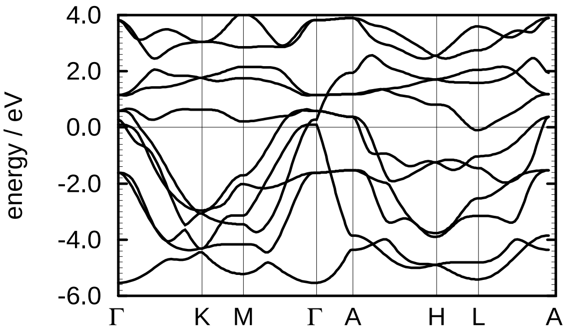

Figure 2: Valence band structure of $TiTe_2$

1.2 Photoemission Theory

Our theory is based on the single particle formalism outlined by Feibelman and Eastman in ref. [3]. The "golden rule" formula for the radial photocurrent measured far outside the sample can be cast into the form

$$I \sim \sqrt{E_{kin}}\,\mathrm{Im}\Big[\sum_{ij}\langle\Phi^{final} \mid \vec{A}\cdot\vec{p} \mid \Psi_i^{initial}\rangle \cdot \cdot \widetilde{G}_{ij}\,\langle\Psi_j^{initial} \mid \vec{A}\cdot\vec{p} \mid \Phi^{final}\rangle\Big] \quad (1)$$

The matrix element $\langle\Phi^{final} \mid \vec{A}\cdot\vec{p} \mid \Psi_i^{initial}\rangle$ is taken between the time inverted LEED state $\Phi^{final} = \Phi^{*}_{LEED}$ and the tight binding Bloch sums $\Psi_i^{initial}$. The vector potential $\vec{A}$ is constant.

The basis $\Psi_i^{initial}$ of the initial states in eq. 1 is calculated using the empirical tight binding method. The surface is properly taken into account by determining the layer and wave vector resolved Green's function G applying a highly convergent renormalization scheme[4]. The tilde denotes the representation in a dual space caused by the nonorthogonality of the basis set.

Within the crystal ($z \leq z_0$) the final states can be written as a superposition of bulk wave functions

$$\Phi^*_{LEED} = \sum_n t_n \, \Phi_n(\vec{k}_n) \quad (2)$$
$$= \sum_n t_n \sum_{\vec{G}} \alpha^{(n)}_{\vec{G}}(\vec{k}_n) \, \exp\left[-i(\vec{k}_n + \vec{G}) \cdot \vec{r}\right]$$

The eigenfunctions $\Phi_n(\vec{k}_n)$ of the Hamiltonian result from the calculation of the complex band structure. To apply the method proposed by Pendry, local atomic pseudopotential coefficients are used[5] which have been evaluated by a local approximation to the nonlocal potentials of ref. [6, 7, 8]. The wave vector component perpendicular to the crystal surface $k_\perp^{(n)}$ is complex in view of the halfspace problem and the damping by an optical potential. Figure 3 shows the complex conduction band structure of $TiTe_2$.

Outside the crystal ($z \geq z_0$) the time inverted LEED state is written as a superposition of plane waves

$$\Phi^*_{LEED} = \exp(i\vec{k}_{\|}\vec{\rho} + i\kappa_0 z) \quad (3)$$
$$+ \sum_{\vec{g}} \phi_{\vec{g}} \, \exp(i[\vec{k}_{\|} + \vec{g}]\vec{\rho} - i\kappa_{\vec{g}} z)$$

The wave vector components perpendicular to the crystal surface depend on the considered beam $\vec{g}$

$$\kappa_{\vec{g}} = \sqrt{\frac{2m}{\hbar^2} E_{kin} - (\vec{k}_{\|} + \vec{g})^2}$$

Since the wave functions have to be smoothly continuous at the plane $z = z_0$, the coefficients t_n and $\phi_{\vec{g}}$ of eq. 2 and 3 can be determined.

2 Many particle effects

In order to take many particle effects in photoelectron spectroscopy into account, selfenergy corrections have to be considered in all one–particle Green's functions. All contributions from electron–electron interactions are included in the complex selfenergy Σ which has to be added to the one–particle energy of the non–interacting system

$$G(E) = \frac{1}{E - H + i\delta - \Sigma(E)}$$

The real part of the selfenergy describing elastic scattering shifts the energy levels whereas the

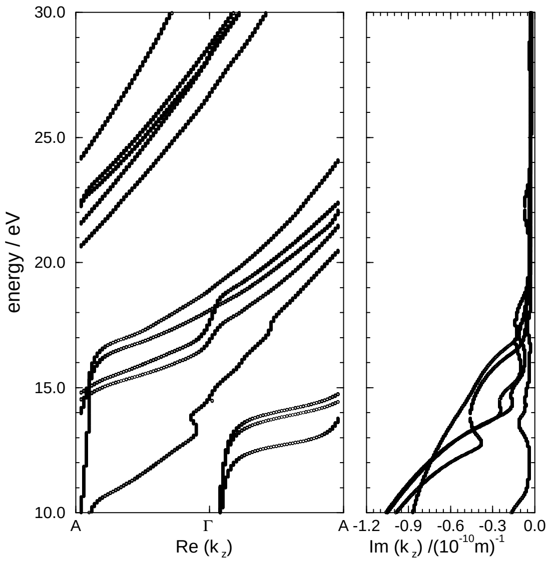

Figure 3: Complex conduction band structure of $TiTe_2$; left panel, real part of perpendicular momentum k_z along $\Gamma - A$, right panel, imaginary part.

imaginary part describing the losses from absorption and inelastic scattering gives an exponential damping of the wave function amplitude.

In this paper we examine separately the influence of many body effects in the initial and in the final states of photoemission. The corrections of the photoemission vertex which previously have been shown to be significant [9, 10] are not included in this paper. They dominantly appear in strong dispersive peaks from orbitals perpendicular to the surface in normal emission and show their signature in a peculiar frequency dependence near the plasma frequency. Those effects may be separated from the present topic of investigation.

2.1 Many particle effects in the final states

Because of the finite lifetime of the escaping photoelectron, photoemission spectroscopy is a surface sensitive experiment. Electrons produced far away from the crystal surface cannot reach the surface and will not contribute to the photocurrent. Therefore the outgoing states in photoemission are localized near the crystal surface and damped inside the the crystal. The following heuristic formula for this damping has shown its usefulness in many calculations of photoemission spectra[11, 12, 13]

$$\mathrm{Im}\,\Sigma^{(e)}(E) = \frac{a}{1+\exp(-(E-\omega_p)/c)} + d \qquad (4)$$

with ω_p being the plasmon frequency (ω_p=18eV [14]). Figure 4 shows the typical shape for $TiTe_2$.

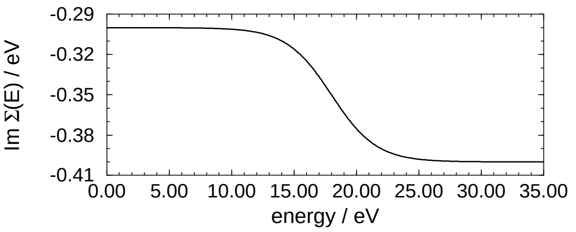

Figure 4: Heuristic damping of the final states with the parameters $a = -0.1$eV, $c = 1.8$eV, $d = -0.3$eV, see eq. 4

In order to consider many particle effects in the final states the heuristic damping should be replaced by the imaginary part of the selfenergy matrix. Much of our present knowledge about the self energy $\Sigma(\vec{k}, E)$ is based on GW calculations[15], i.e. vertex corrections being neglected, as in

$$\Sigma^{(e)}(\vec{r}, \vec{r}\,', E) = \frac{i}{2\pi} \int dE'\; e^{iE'\delta}\; G(\vec{r}, \vec{r}\,', E+E')\; W(\vec{r}, \vec{r}\,', E')$$

This formula requires the Green's function G and the dynamically screened interaction $W = \epsilon^{-1}V$. We have to consider the dielectric matrix as diagonal because only the frequency dependence is available for $TiTe_2$[14]

$$\epsilon^{-1}_{\vec{G}\vec{G}'}(\vec{k}, E) = \epsilon^{-1}(E) \cdot \frac{(\vec{k}+\vec{G})^2}{(\vec{k}+\vec{G})^2 + \kappa^2_{TF}}\; \delta_{\vec{G}\vec{G}'} \qquad (5)$$

To account for the long wavelength screening a Thomas–Fermi cut–off with $\kappa_{TF} = 1.55\text{Å}^{-1}$ has been used.

Finally, the following expression for a diagonal matrix element of the selfenergy matrix is obtained

$$\Sigma^{(e)}_{\vec{G}\vec{G}}(\Gamma, E) = \frac{i}{(2\pi)^4} \sum_{\vec{G}'} \int_{BZ} d\vec{k}' \int dE'\; e^{iE'\delta} \cdot$$
$$\cdot G_{\vec{G}'\vec{G}'}(\vec{k}', E+E')\; W_{\vec{G}-\vec{G}',\vec{G}-\vec{G}'}(-\vec{k}', E')$$

Only the $\vec{k} = 0$ correction from Σ, i.e. that at the Γ–point, may be applied because a local potential is needed for our complex band structure scheme. The method of special points is used for the Brillouin zone integration. For illustration the shape of four matrix elements is shown in figure 5.

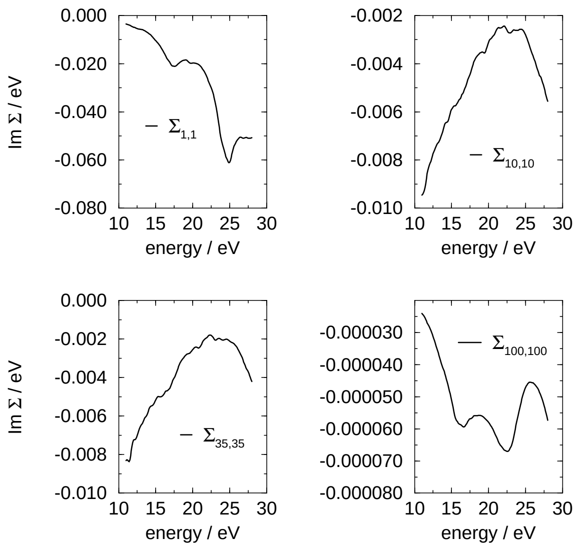

Figure 5: Energy dependence of four typical GW matrix elements, calculated with 11613 special points in the Brillouin zone; $\Sigma_{1,1}$ stands for the $(\vec{G}, \vec{G}') = (0, 0)$ matrix element.

Figure 6 shows calculated and experimental [16] spectra for the ΓA–direction. The theoretical spectra were evaluated by applying the heuristic damping (dashed lines) and the damping by the imaginary part of the GW selfenergy (solid lines). In principle, the solid and dashed curves show photoemission maxima for the same binding energies, but the peak heights strongly differ. The order of magnitude of the selfenergy matrix element $\Sigma_{1,1}$ is approximately one tenth of the heuristic damping explaining the sharp peaks of the solid curves. For higher frequencies the experimental peak widths are in favor of a larger theoretical broadening. However, a constant damping as in the dashed curves is clearly not adequate.

For photon energies below 20eV, the difference between the solid and the dashed curves is rather small. The relative peak height of the dominating peak dispersing from -1.9eV to -3eV is more pronounced in comparison with the experiment. For photon energies above 20eV, there are distinct differences between the solid and the dashed curves. Both are lacking the dominance of the experimental peak near the Fermi edge for pho-

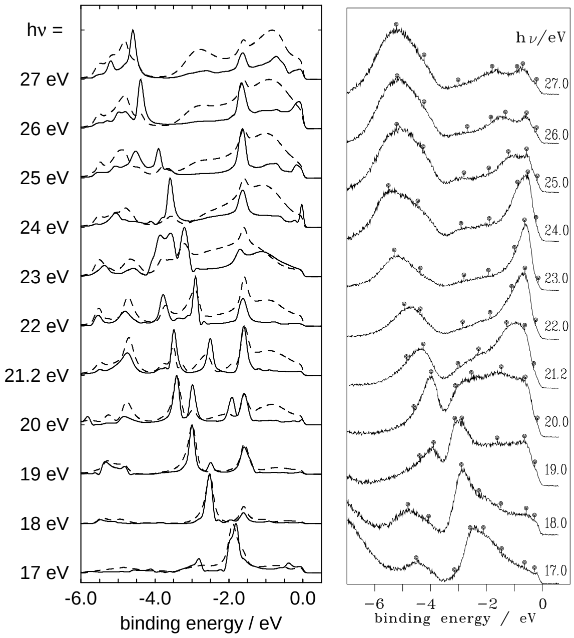

Figure 6: Photocurrent vs. binding energy, theoretical (left) and experimental (right) ΓA spectra for an angle of incidence of $\xi = 45^o$. The dashed curve belongs to the heuristic damping, the solid curve to the selfenergy damping.

ton energies between 20eV and 24eV. For photon energies above 23eV, the solid curves are clearly closer to experiment than the dashed curves, e.g. in experiment the peaks below -3.5eV are higher than those above -3.5eV, and the peaks between 0eV and -2eV form a plateau–like shape. There are possible explanations for only a partial success of the GW selfenergy damping. The approximative treatment of the $\vec{k}$–dependence in eq. 5 and κ_{TF} too large may underestimate the broadening. The neglect of the photon screening by the electron system underestimates the heights of some dispersive peaks, as e.g. the peaks leading to the experimental maximum near -5eV[9, 10].

2.2 Many particle effects in the initial states

Electron–electron correlation may lead to a characteristic variation of the photoemission line shapes in metals and high temperature superconductors solely based on a Fermi liquid behavior of the spectral function. Line shape analysis of experimental $TiTe_2$ photoemission spectra has been performed along the ΓM direction within

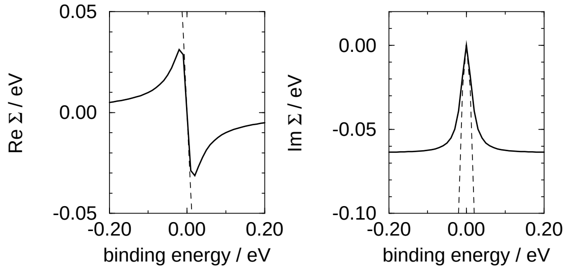

Figure 7: Real (left) and imaginary (right) part of the selfenergy for $Q = 1$, $Z_F = 0.2$ and $\beta = 250 eV^{-1}$ using eq. 7 (solid lines) and eq. 6 (dashed lines)

this frame[1, 2].

From general considerations Luttinger proposed the following formula for the selfenergy of the three dimensional Fermi liquid[17]

$$\Sigma^{(h)}(E) = \alpha E - i\beta E^2 \tag{6}$$

Since this approximation is valid only for small values of E in the immediate neighbourhood of the Fermi energy, Matho suggested a corrected selfenergy in a comment[18] on the work of Claessen et al.[1]

$$\Sigma^{(h)}(E) = \frac{(Q - Z_F)^2}{Q^2 Z_F^2 \beta^2 E^2 + (Q - Z_F)^2} \cdot \left[\left(1 - 1/Z_F\right) E - i\beta E^2 \right] \tag{7}$$

with $Z_F = \frac{1}{1-\alpha}$ and $Z_F < Q \leq 1$.
In ref. [1] and [2] the authors use $Q = 1$, $Z_F = 0.2$ and $250\, eV^{-1} < \beta(\vec{k}_\parallel) < 430\, eV^{-1}$. In each of the spectra shown below as well as in the experimental spectra[2] β is taken as a constant over the plotted binding energy range of 0.4eV. Figure 7 shows the typical shape of $\Sigma^{(h)}$ evaluated with eq. 6 and 7.

For the calculation of the photoemission spectra we finally consider eq. 7 as an approximation of the initial state selfenergy and adequately choose the above parameters. The final state selfenergy is rather constant over such a small energy interval and may be safely approximated by a constant optical potential in accordance with the GW results of the last section.

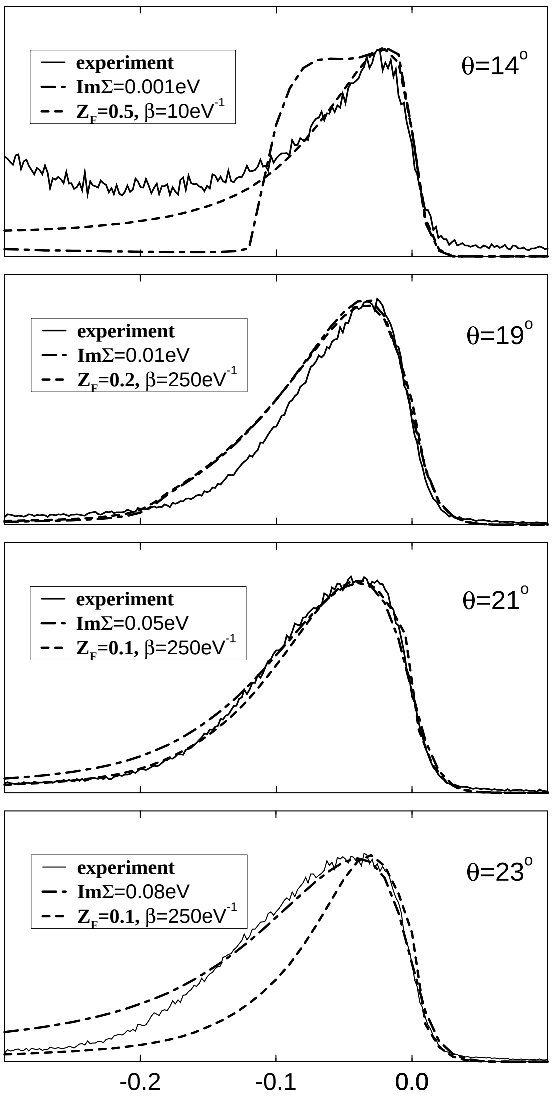

Figure 8: Photoemission spectra along the ΓM direction near the Fermi edge, calculated data using eq. 7 (dashed lines) and using a constant, purely imaginary selfenergy (dot–dashed lines), and experimental data (solid lines).

Figure 8 shows four photoemission spectra along the ΓM direction near the Fermi edge. Each panel contains the experimental curve and two calculated curves, one using eq. 7 and one using a constant, purely imaginary selfenergy. With increasing values of θ, the success of applying the Fermi liquid model (eq. 7) obviously decreases. For $\theta = 14^o$, using eq. 7 improves the agreement with experiment noticeably over taking a simply constant selfenergy. For all other θ's the use of a constant, purely imaginary selfenergy is as good (e.g. for $\theta = 21^o$) as or even better (e.g. for $\theta = 23^o$) than the use of eq. 7 for the selfenergy. This means that the parametrization of the Fermi liquid selfenergy of eq. 7 is only suitable in a very narrow region where the Ti–3d derived band crosses the Fermi level. This angular range appears to be still smaller than that found by direct fitting of the spectral density to the spectra in ref. [2]. The peculiar shape of the dot–dashed curve for $\theta = 14^o$ originates from a second band above the Fermi level. Its tail is seen in emission. It is not cut off by the narrow line width of the Fermi liquid as reflected by the dashed curve. In so far this result can be interpreted as a strong hint for a Fermi liquid behavior.

3 Conclusions

The normal emission spectra calculated in the onestep model for $TiTe_2$ are in reasonable agreement with experiment. The GW–approximation for the final states slightly improves the agreement, though it underestimates the damping at higher frequencies a little. In nonnormal emission the behavior of the valence spectral density near the Fermi edge is tested. Within a small energy and angle interval, where the peak remains close to the Fermi level, a Fermi liquid behavior seems to be confirmed.

Acknowledgements

We are indebted to Dr.E.E. Krasovskii for providing us with the calculated $\epsilon(E)$ data prior to publication. This work is financially supported by a grant of the Land Schleswig–Holstein and by the Bundesministerium für Bildung und Forschung, contract no. 05 605 FKA.

References

[1] R. Claessen, R. O. Anderson, J. W. Allen, C. G. Olson, C. Janowitz, W. P. Ellis, S. Harm, M. Kalning, R. Manzke and M. Skibowski, *Phys. Rev. Lett.* **69**, 808 (1992).

[2] S. Harm, R. Dürig, R. Manzke, M. Skibowski, R. Claessen and J.W. Allen, *J. Electron. Spectrosc. & Relat. Phenom.* **68**, 111 (1994).

[3] P.J. Feibelman and D.E. Eastman, *Phys. Rev. B* **10**, 4932 (1974).

[4] J. Henk and W. Schattke, *Comp. Phys. Commun.* **77**, 69 (1993).

[5] J.B. Pendry, *J. Phys. C* **2**, 2273 (1969).

[6] D.R. Hamann, M. Schlüter and C. Chiang, *Phys. Rev. Letters* **43**, 1494 (1979).

[7] G.B. Bachelet, D.R. Hamann and M. Schlüter, *Phys. Rev. B* **26**, 4199 (1982).

[8] D.R. Hamann, *Phys. Rev. B* **40**, 2980 (1989).

[9] D. Samuelsen, E. Pehlke, W. Schattke, O. Anderson, R. Manzke and M. Skibowski, *Phys. Rev. Letters* **68**, 522 (1992).

[10] D. Samuelsen and W. Schattke, *Surf. Sci.* **327**, 379 (1995).

[11] T. Grandke, L. Ley and M. Cardona, *Phys. Rev. B* **18**, 3847 (1978).

[12] J. Henk, W. Schattke, H. Carstensen, R. Manzke and M. Skibowski, *Phys. Rev. B* **47**, 2251 (1993).

[13] E. Pehlke, W. Schattke, O. Anderson, R. Manzke and M. Skibowski, *Phys. Rev. B* **41**, 2982 (1990).

[14] E.E. Krasovskii, calculation of $\epsilon(E)$ with an extended LAPW scheme, *private communication.*

[15] L. Hedin and S. Lundquist, *Solid State Physics* **23**, 1 (1969).

[16] S. Harm, *Thesis,* Kiel, (1994).

[17] J.M. Luttinger, *Phys. Rev.* **121**, 942 (1960).

[18] K. Matho, *unpublished* .